Research Article

Glass beads immobilized doped TiO_2 NPs with enhanced adsorption efficiency for arsenic(III) from aqueous solution

Najm Us Saqib[1,2] · Ajmal Khan[1] · Israr Alam[1] · Muhammad Rahim[2]

Received: 6 January 2020 / Accepted: 6 February 2020 / Published online: 12 March 2020

Abstract
Visible light driven metals (Gd and Tl) doped TiO_2 nanoparticles (NPs) were prepared using low cost and facile liquid impregnation method. The prepared NPs were characterized using XRD, SEM/EDX, BET surface area analysis, particle size distribution analyzer, UV–Vis DRS and pH of point of zero charge (pH_{PZC}) analyses. The crystalline phases observed were purely anatase with the particles size ranged between 24 and 30 nm possessing large surface area (74 m^2/g) and pore size (12 nm). The reductions in the band gap energy for both the dopant systems were observed and absorption edges were extended to the visible region. The prepared NPs exhibited good photo-induced adsorption affinity for the As(III) from aqueous solution under natural pH of As(III) solution, ambient temperature and normal household compact fluorescent light. The metals-doped NPs showed high removal efficiency (up to 99%) towards As(III) compared to pure TiO_2 NPs (68%). In addition, the glass beads immobilized photocatalyst not only enhanced the efficiencies by increasing the active surface area of NPs, but also overcome the post-reaction separation steps. The regeneration study indicated that the physical regeneration is more significant for the reutilization of photocatalysts.

Keywords Titanium dioxide · Doping · Immobilization · Arsenic(III) · Adsorption

1 Introduction

Arsenic and its compounds are well known for their toxicity and carcinogenic effects. The increase in arsenic exposure to human population has been observed when people started using underground water in preference to surface water contaminated with micro-organisms [1]. Contamination of arsenic in groundwater has become a global issue and has brought serious health problems such as skin cancers, bladder diseases and kidney failure in human [26]. Millions of people from India, China, Bangladesh, Pakistan, Australia and South America are exposed to arsenic by consuming drinking water where its concentration exceeded the maximum permissible limit (10 µg/L) [5, 23, 26]. Arsenic is classified as a Class I human carcinogen by the International Agency for Research on Cancer (IARC) due to its association with many adverse human effects [3]. The toxicity of As(III) is reported about 25–60 times higher than that of As(V) [13]. Meanwhile, As(III) show a low adsorption performance to various adsorbents compared to As(V) [26]. Generally, As(III) exists in anaerobic waters while As(V) present in aerobic waters [8, 25]. Commonly used technologies for the removal of arsenic from drinking water including separation processes (i.e. coagulation/filtration), ion exchange and adsorption, however, the disposal of arsenic-bearing wastes obtained from these methods are serious problems [4, 8]. Therefore, pretreatment such as oxidation of As(III) to the less toxic As(V) are usually required for the adsorption removal processes. Different oxidants such as O_3, H_2O_2, MnO_2, chlorine, chlorine dioxide, dichloroamine ($NHCl_2$), and ferrate (FeO_4^{2-}) were previously used for the oxidation of As(III) to As(V)

✉ Najm Us Saqib, najam@ubuner.edu.pk | [1]Department of Zoology, University of Buner, Buner, KP, Pakistan. [2]School of Chemical Sciences, Universiti Sains Malaysia, 11800 George Town, Penang, Malaysia.

[8, 26]. Unfortunately, conventional oxidants, especially chlorine, chlorine dioxide and ozone resulting in various drawbacks including limited removal efficiency, expensive reagents and dangerous oxidation by-products [20].

Adsorption process is considered to be the best available technique for the removal of arsenic. Heterogeneous photocatalysis, using TiO_2 NPs has been used as an alternative for the adsorption of arsenic from drinking water [8]. Previously reported study indicated that modified TiO_2 NPs not only adsorb both the species but also photo-oxidizes As(III) species to As(V) followed by adsorption [2, 8, 26]. Titania nano-catalyst showed greater affinity towards the adsorption of As(III). Titanium dioxide NPs were first time investigated by Jezequel and Chu [11], for its potential to remove arsenic showing promising results. Deedar and Aslam [6], evaluated the arsenic removal potential of TiO_2 NPs by immobilizing onto sand. The works Miller and Zimmerman [18] showed that TiO_2 impregnated on chitosan beads successfully posed their arsenic sorption ability as a photocatalytic sorbent. Doped TiO_2 being a good light induced photocatalyst over a wide range of pH (2–14) showed good affinity towards arsenic adsorption [5].

Titanium dioxide NPs have been recognized to be the best photocatalyst among other semiconductors due to its less toxicity, eco-friendly nature, low cost, high efficiency, oxidizing photo-generated holes and high stability in wide pH range [21]. However, the fundamental limits with TiO_2 NPs are the wide band gap energy of 3.20 eV, which can only be activated in UV light, and the transitions from anatase to rutile phase. In order to reduce the electron-hole recombination and to shift the absorption wavelength to desired visible region, various metals and non-metals doping modifications have been used [5, 8, 21].

Generally, in photocatalytic processes the removal of pollutants using semiconductor NPs were employed in a suspension, however, it may not be possible to completely recover the NPs used in the reactions. Similarly, the separation of NPs (TiO_2) from the liquid phase, in order to recycle them, is practically a lengthy and difficult process [22]. Therefore, numerous of researchers studied the feasibility of coating/immobilizing the photocatalyst on to inert solid substrate such as porous ceramic surfaces, chitosan beads, glass beads, zeolite and activated carbon [12, 18, 22, 24, 26, 29]. Immobilization of the nano-catalyst on a solid support could avoid the need to recover the NPs from the reaction mixture without any leaching.

The main objective of the present study is to prepare Gd/TiO_2 and Tl/TiO_2 NPs using a facile method of preparation, and to reduce the barrier of UV irradiation requirement by shifting the absorption edges to longer wavelength (visible light). The prepared photocatalyst was further applied for the removal of As(III) from aqueous solution. The adsorption study was performed at neutral pH of solutions under compact fluorescent light. The adsorption efficiency of NPs was investigated for the removal of As(III) from aqueous solution exposed to compact fluorescent light. The pure and metal doped TiO_2 were immobilized on glass beads (2 mm) by heat attachment method, to avoid agglomeration and to easily separation doped NPs.

2 Materials and methods

2.1 Materials

General purpose reagent (GPR) amorphous titanium(IV) oxide (BDH Chemicals Ltd., England) and nitrate salts of different metal i.e. gadolinium(III) nitrate hexa-hydrate and thallium(III) nitrate tri-hydrate, NaOH and HNO_3 (Merck, Germany) were used in this study. All chemicals were of analytical grade and were used without further purification. De-ionized water prepared by Deionizer Water Pro Polishing Station LABCONCO was used as a solvent for all solutions.

2.2 Preparation of metals doped TiO_2 NPs

Gd and Tl doped TiO_2 NPs were prepared by liquid impregnation (LI) method using the following procedure [22]. GPR TiO_2: 5 g was slowly added to 100 mL deionized water with continuous stirring and the required amount of all the metals salts were mixed to the TiO_2 suspension, separately. The salts concentration was kept 1 M% with respect to TiO_2. The slurry was stirred for 12 h and settle down for 12 h. Later, the slurry was then dried in an oven for 12 h at 100 °C. The dried samples were ground in agate mortar and were calcined at 400 °C for 6 h in a furnace.

The mass percent yield of doped and pure TiO_2 using LI method with GPR titanium(IV) oxide precursor was up to 95%, calculated by using the following equation:

$$\text{Percent yield } (\%) = \frac{\text{Actual yield}}{\text{Theoretical yield}} \times 100 \quad (1)$$

Heat attachment method was used to immobilize TiO_2 on glass beads (2 mm diameter) [12]. The glass beads were etched by using NaOH (1:20 v/v) for 24 h and then washed vigorously with deionized water. TiO_2 powder slurry was prepared, by mixing of pure and metal doped TiO_2 in of deionized water separately, and was thoroughly dispersed using orbit shaker. The glass beads were immersed in the slurry of TiO_2, and were mixed by stirring at the speed of 400 rpm for 2 h. The suspension was removed and then placed in an oven for 1.5 h at 150 °C and were calcined in

a furnace for 2 h at temperature of 400 °C. The glass beads samples were then washed with double distilled water to remove the loosely attached TiO_2 particles.

2.3 Characterizations

Powder X-ray diffraction analysis was used to study the crystal phase composition and crystallite size of the prepared NPs. XRD patterns were obtained on Panalytical Antonpar 3040/60 Xpert Pro XRD Diffractometer, using Cu-K_α radiation at an angle of 2θ ranged from 20° to 80°. The crystallite sizes were determined from the X-ray diffraction patterns, based on the Debye–Scherrer equation [16]:

$$D = \frac{k\lambda}{\beta \cos\theta} \tag{2}$$

where k is a shape factor = 0.9, λ is the radiation wavelength = 1.54051 Å, β = full width of a diffraction line at one half of maximum intensity in radian. The crystallite phase compositions were calculated using Eq. 3 [10]:

$$W_A = \frac{k_A A_A}{k_A A_A + A_R + k_B A_B} \tag{3}$$

where A_A, A_B, and A_R are the integrated intensities of the anatase (1 0 1), brookite (1 2 1), and rutile (1 1 0) peaks. The values of k_A and k_B are 0.886 and 2.721, respectively [10].

Scanning electron microscopic (SEM) study of pure and doped TiO_2 NPs was conducted with JEOL JED-2300 scanning electron microscope to observe the surface morphology of TiO_2. Energy dispersive spectroscopic analysis (EDX) was conducted with EDX system embedded with JEOL JED-2300 SEM unit to perform the quantitative analysis of powder and glass beads coated TiO_2 NPs. Total surface area is measured from the quantity of sample material required to form a single layer (a monolayer) on sample surface. The total surface area is calculated from the known area per molecule or ion adsorbed. In this study, the BET (Brunauer–Emmett–Teller) pore diameter and specific surface area of pure and doped TiO_2 NPs were analyzed by NOVA WIN 2200e Surface and Pore Size Analyzer. To know the dispersion of NPs in the process of adsorption, the average particle size and particle size distribution of the nanoparticle powders were determined in water medium using a light scattering particle analyzer in the range of 0.110–200 µm (Horiba Particle Size Analyser LA-300). The NPs powder was ultrasonically dispersed in deionized water for 3 min prior to examination of particle distribution via light scattering particle analyzer. To find the band gap energy of semiconductor photocatalyst required specific excitation wavelength of light required. The diffused reflectance of pure and doped TiO_2 samples was analyzed by using PerkinElmer, LAMBDA 35 UV/Vis spectrophotometer. The electronic properties of the prepared NPs were investigated using the remission function of Kubelka–Munk, (R_∞) [7, 27].

$$F(R_\infty) = \frac{(1 - R_\infty)}{2R_\infty} \tag{4}$$

The pH_{PZC} of pure and doped TiO_2 NPs were determined by a modified pH drift method [22]. Generally, the initial pH of 0.1 M $NaNO_3$ solutions were adjusted to 2 to 12 using 0.01–0.1 M HNO_3 or NaOH solutions. Subsequently, 0.1 g of the NPs were added and equilibrated for 24 h. The final pH of each system was determined and the difference between the initial and final pHs (ΔpH) was plotted against the initial pH. The pH values at which the curve crosses zero, was taken as the pH_{PZC} of the material.

2.4 Removal efficiency

The stock solution of arsenic(III) (1000 mg/L) was prepared by adding 300 mL of sodium arsenite aqueous solution (1 mL = 0.006495 mg $NaAsO_2$ MERCK Germany). The solution was mixed using sonicator. The pH of the solution was adjusted to 7.0 ± 0.1 by adding HNO_3 (MERCK Germany) and the sample was purged with nitrogen gas. After overnight mixing, it was stored in dark. The removal efficiency (E%) of pure and modified TiO_2 NPs were measured using the following equation:

$$E(\%) = \frac{C_o - C_f}{C_o} \times 100 \tag{5}$$

where C_o and C_f are initial and final equilibrium concentrations of As(III) (mg/L) in aqueous solution, respectively. Quantitative determination of As(III) was carried out by using AAS Vario 6, analytikjena (Germany) in hydride generation mode. For analysis, 0.2 g of TiO_2 NPs was used in 80 ml of 0.5 mg/L solution of As(III) solution was taken in 250 mL flask. The solutions were centrifuged at 5000 rpm for 5 min to remove powder NPs. After centrifugation, the collected solutions were preserved with standard 1:1 solution of conc. HNO_3. The preserved samples were analyzed with AAS Vario 6, Analytikjena (Germany). However, no centrifugation step was performed after immobilized samples adsorptions. Batch test was performed by using 80 mL of As(III) solutions of different initial concentrations (0.1, 0.2, 0.3, 0.4, 0.5, 1, 1.5, 2 and 5 ppm) were mixed with

0.2 g with both pure and doped TiO_2 NPs. The orbit shaker with 120 rpm speed was used for the 1 h to ensure the complete adsorption.

2.5 Regeneration of photocatalyst

Regeneration ability of the used photocatalysts was examined via high temperature combustion method with slight modifications [22]. The spent photocatalyst samples were filtered and stirred in 2 M NaOH solution for 20 min. The samples were washed properly with deionized water and dried in an oven for 100 °C. The samples collected were exposed to high calcination temperature treatment (400 ± 20 °C) in a furnace with a heating rate of 5 °C/min for 3 h. The reusability of each sample was investigated up to three numbers of cycles upon continuous use.

Table 1 Physico-chemical properties of pure and doped TiO_2 NPs

NPs	TiO_2	Gd–TiO_2	Tl–TiO_2
Average size (nm)	30.0	24.3	28.2
Anatase phase (%)	100	100	100
Surface area (m^2/g)	50.1	73.6	60.3
Pore volume (nm)	11.2	12.1	12.0
pH_{PZC}	6.61	6.40	6.32
Band gap energy (eV)	3.20	3.08	3.01

3 Results and discussion

3.1 Crystal phase composition of TiO_2 NPs

X-ray diffraction technique was used to investigate the crystallite size and the crystal phase composition of pure and metals doped TiO_2 NPs. The X-ray diffraction pattern of pure, Gd and Tl doped TiO_2 (calcined at 400 °C) were found similar and containing pure anatase phase and no rutile or brookite reflection was observed in JCPDS Card Number 73-1764. The average crystallite size of pure and doped TiO_2 NPs calculated using Eq. 2, is given in Table 1. It was observed that doping slightly decrease the particles size. The particles were exposed to 400 °C annealing treatment and it was found advantageous to get fine anatase phase with greater surface area and good photocatalytic property. Similarly, the previous studies indicated that doping with lanthanide metal reduces anatase to rutile phase transformation [19, 21] (Fig. 1).

3.2 SEM/EDX analyses

Scanning electron microscopic technique was used for the direct observation of particle size and morphology of the sample powders. Samples were consisted of more fine particles (microparticles) and most of the particles were spheroid or oblate spheroid and loosed shaped particles. Figure 2 shows the glass beads coated doped and pure TiO_2

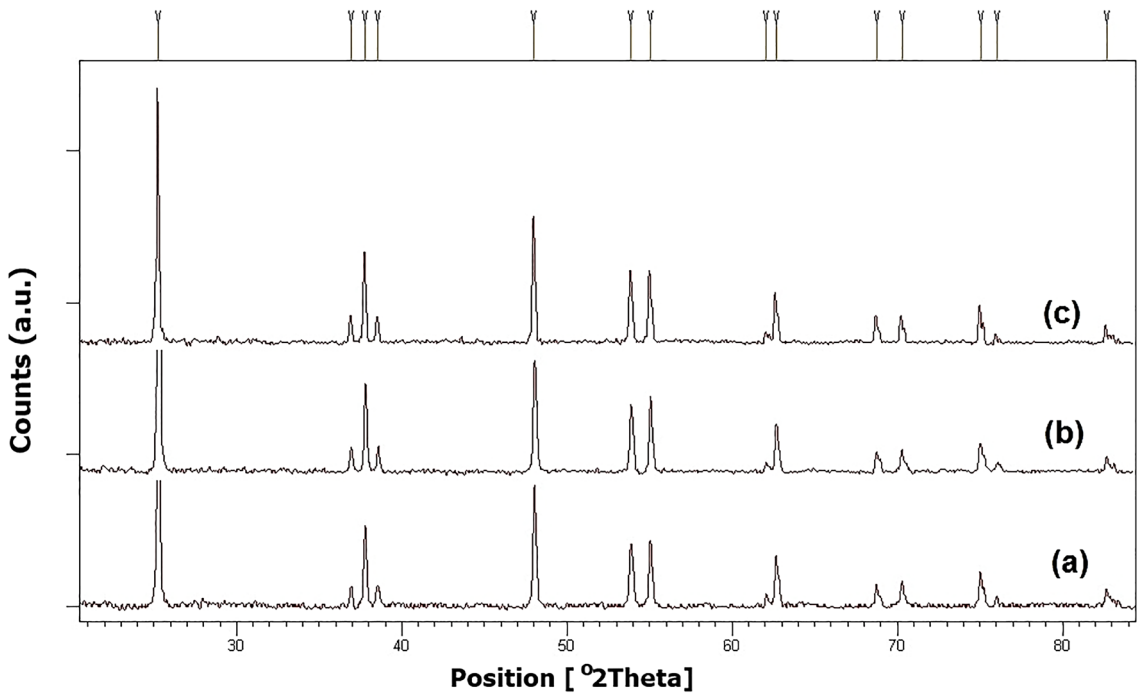

Fig. 1 XRD pattern of pure and doped TiO_2 NPs (a) Gd/TiO_2, (b) Tl/TiO_2, and (c) TiO_2 NPs, respectively calcined at 400 °C

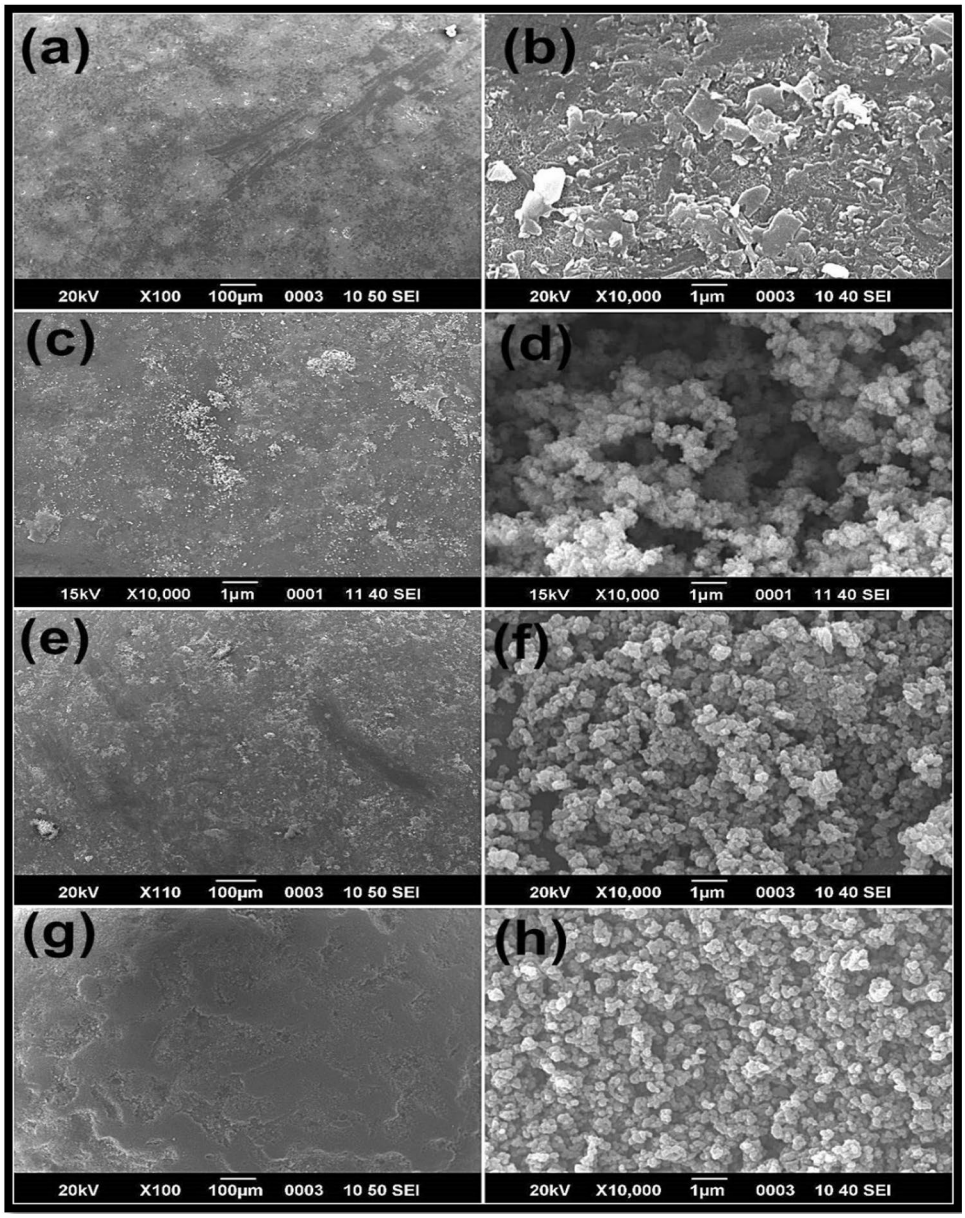

Fig. 2 SEM micrographs at different resolutions of **a**, **b** glass beads, and etched glass beads **c**, **d** pure TiO_2, **e**, **f** Gd/TiO_2, **g**, **h** Tl/TiO_2, respectively

NPs. It was observed that in the coated sample the NPs have almost same morphology as that of powder samples. Figure 2, illustrates the different resolutions SEM micrographs of glass beads, TiO_2-coated glass beads and doped TiO_2-coated glass beads. The SEM results indicated that the NaOH etching of glass beads increase the roughness of glass beads surface which favors the attachment of NPs on the surface. Pure TiO_2 exist in agglomerates form on the surface of glass beads, however, Gd and Tl doped TiO_2 present in well dispersed manners. Previously reported studies also indicated that the doping with lanthanides metals increase the dispersion of TiO_2 NPs as compared to pure TiO_2, whereas the tiny particles agglomerates [17, 19].

The elemental composition of powder and glass beads coated doped and pure TiO_2 NPs was analyzed by EDX technique, as shown in Table 2. The EDX results showed different percentage covering of for pure and doped system on the surface of glass beads. The glass beads surface covering of Tl/TiO_2 was observed higher than Gd/TiO_2 and pure TiO_2, which signify the enhancement in removal efficiency of the immobilized Tl/TiO_2.

3.3 BET and BJH analysis

Surface area and pore size/volume were determined by BET and BJH isotherms methods respectively using nitrogen adsorption-desorption. The surface area Gd/TiO_2 and Tl/TiO_2 NPs were 73.6 and 60.3 m^2/g, while nanopores were present in the NPs with diameter in the range of 12.1 and 12.0 nm, respectively as shown in the Table 1.

Table 2 EDX elemental surface composition of powder and glass beads immobilized pure and doped TiO_2 NPs

NPs	Without glass beads (Mass %)				With glass beads (Mass %)				
	Ti	O	Gd	Tl	Ti	O	Gd	Tl	Si
TiO_2	46	53	–	–	24	44	–	–	30
Gd/TiO_2	47	51	1.0	–	12	49	0.4	–	34
Tl/TiO_2	46	52	–	1.2	38	46	–	0.6	12

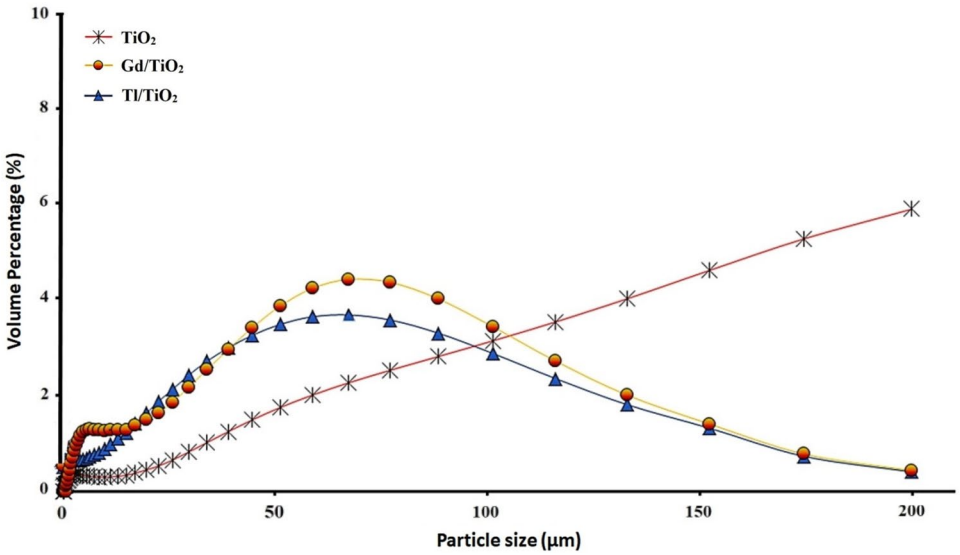

Fig. 3 Particle size distribution of the powder pure and doped TiO_2 NPs within water after 3 min of ultrasonic dispersion

The BET isotherms shows distinctive cylindrical pores and mesoporous structure, and not much more micro-porosity in doped TiO_2 NPs were observed. The average pore diameter shows that most of the pores are mesopores and should imitate the inter-particle porosity in the doped TiO_2 NPs aggregates. By comparing the results to pure TiO_2 NPs (50 m^2/g), the relative high surface areas were observed for the of doped samples. This may be due to the formation of metal TiO_2 composites oxides, which effectively enhanced the surface area of doped TiO_2 NPs [19].

3.4 Particle size distribution

In heterogeneous photocatalysis the dispersion of NPs powder in the slurry reaction system is very important. The particle size distributions of the prepared NPs were detected with water medium after 3 min of ultrasonic dispersion. The results indicate that the doped TiO_2 NPs has almost the same particle size distribution in water, as shown in Fig. 3. However, for pure TiO_2 NPs the volume percentage of larger particles were higher, which indicate the aggregation of pure TiO_2 NPs in aqueous system. The lanthanide ions (La^{+3})-doped titania avoid agglomeration in aqueous medium [28]. Similar behavior of Gd and Tl doped TiO_2 NPs indicates that both of the dopants system increased the dispersion of NPs in aqueous medium,

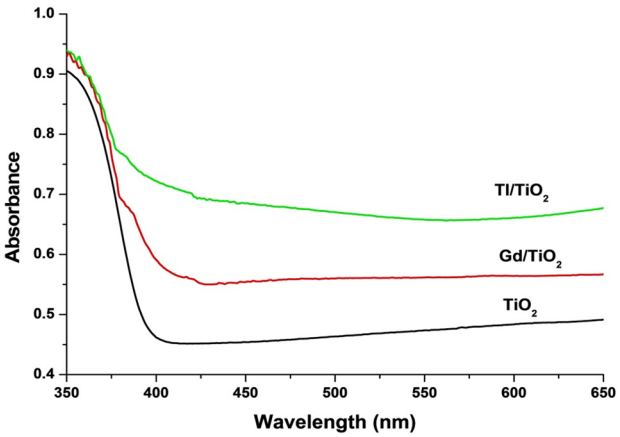

Fig. 4 DRS UV–Vis absorbance spectra of pure and doped TiO_2 NPs

resulting an increased As removal efficiency compared to pure TiO_2 NPs.

3.5 UV–vis DRS analysis

UV–vis DRS spectra of pure and doped TiO_2 is shown in Fig. 4. It was observed that the absorption edges of Gd and Tl doped TiO_2 shifted towards longer wavelength (red shift) compared to pure TiO_2 NPs, which illustrates that the

samples are active in normal visible light (compact fluorescent light). The band gap energy (E_g) of pure and doped TiO_2 NPs were calculated from the plot of $F(R)^{1/2}$ versus E for indirect transition [27], the values are given in Table 1.

4 Removal efficiency

4.1 pH of point of zero charge (pH_{PZC}) and effect of pH on the removal of As(III)

Figure 5a illustrate the results of the pH drift method for the pH_{PZC} values of pure and doped TiO_2 NPs. The values at which $pH < pH_{PZC}$, means the TiO_2 surface having net positive charge, whereas at $pH > pH_{PZC}$ the TiO_2 surfaces were negatively charged. The comparative pH_{PZC} values are given in Table 1. The results indicate that the pH_{PZC} of doped TiO_2 slightly decrease compared to pure TiO_2 NPs.

The effect of pH values on arsenic removal is shown in Fig. 5b. It was observed that with the increase in pH from 4 to 7 the efficiency increases, however decrease in efficiency was observed at pH 10. Adsorption of As(V) is a pH dependent process. Previous study indicated that the adsorption of As(V) was higher in acidic pH (pH < 8), while the pH of the solution had no influence on the adsorption of As(III) [14]. Iervolino et al. [8] observed that the complete adsorption of As(V) on the surface of $MoOx/TiO_2$ did not occur until the complete photocatalytic oxidation of As(III) to As(V). In addition, the present results also indicate the higher pH favors the photocatalytic oxidation of As(III) to As(V) which subsequently reduces the adsorption efficiency of TiO_2 NPs. Therefore, the pH 7 ± 0.02 was selected for the adsorption of As(III) in the present work.

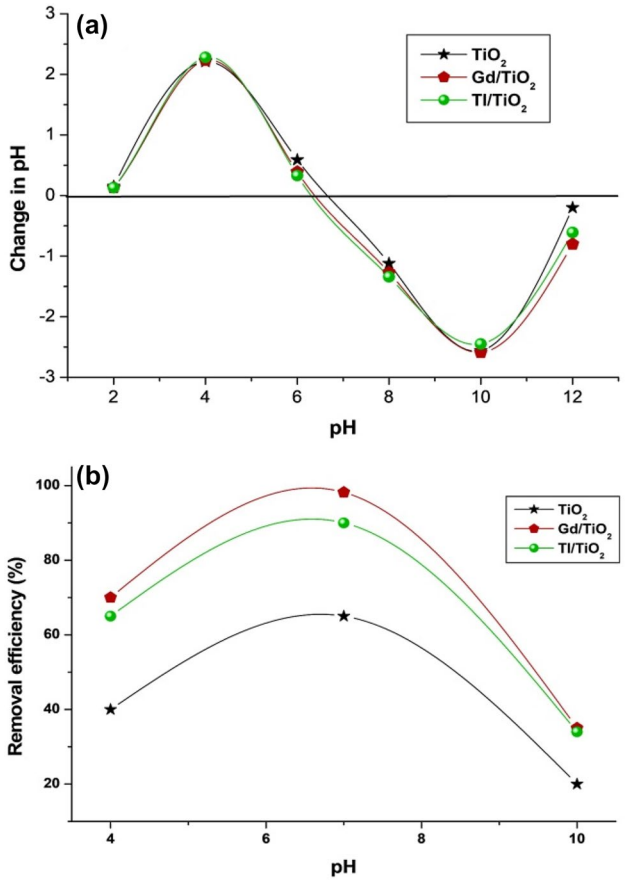

Fig. 5 **a** pH of point of zero charge, and **b** effect of pH on the adsorption of As(III) onto pure and doped TiO_2 NPs

4.2 Adsorption isotherms study

To investigate the adsorption capacity of the pure and doped TiO_2 NPs Langmuir and Freundlich isotherm models were applied to the experimental data obtained from the removal of different initial As(III) concentration (0.1–5 mg/L). The Langmuir isotherm model show the monolayer adsorption occurs at fixed number of localized sites on the surface of adsorbents. The Langmuir adsorption isotherm is based on the assumptions of a structurally homogenous adsorbent, and is shown by the following equation [9]:

$$\frac{C_e}{q_e} = \frac{C_e}{q_m} + \frac{1}{q_m b} \tag{6}$$

where C_e (mg/L) is the equilibrium concentration in the solution, q_e (mg/g) is the amount of As(III) adsorbed per unit weight of adsorbents at specified equilibrium, q_m (mg/g) is the maximum adsorption at monolayer coverage and b (L/mg) is the Langmuir constant related to energy of adsorption which quantitatively shows the affinity of binding sites.

The dimensionless constant separation factor or equilibrium parameter R_L explains the essential characteristic of Langmuir isotherm model [9] which is defined by Eq. 7:

$$R_L = \frac{1}{1 + bC_o} \tag{7}$$

where b (L/mg) is Langmuir constant, and C_o (mg/L) is the initial concentration. The mathematical calculations show that the parameter R_L indicates the shape of isotherms. The classified R_L value as $0 < R_L < 1$, suggest whether the adsorption is unfavorable, favorable and irreversible respectively [9]. The R_L values calculated from present results indicate that the adsorption is favorable (Table 3).

The linear Langmuir adsorption isotherms of pure and doped TiO_2 are illustrated in Fig. 6. The Langmuir parameters, q_m and b, calculated from the slope and intercept of the graphs and are given in Table 3.

Table 3 Adsorption isotherms parameters of As(III) adsorption onto pure and doped TiO_2 NPs at 25 ± 2 °C

NPs	Langmuir model					Freundlich model		
	q_m, *Exp* (mg/g)	q_m, *Cal* (mg/g)	*b* (L/mg)	R_L	R^2	*n*	K_f	R^2
TiO_2	0.92	1.03	0.89	0.91–0.18	0.990	2.4	0.87	0.745
Gd/TiO_2	2.76	2.96	0.90	0.99–0.68	0.995	1.7	0.72	0.851
Tl/TiO_2	2.41	2.61	0.59	0.99–0.77	0.999	2.0	0.91	0.876

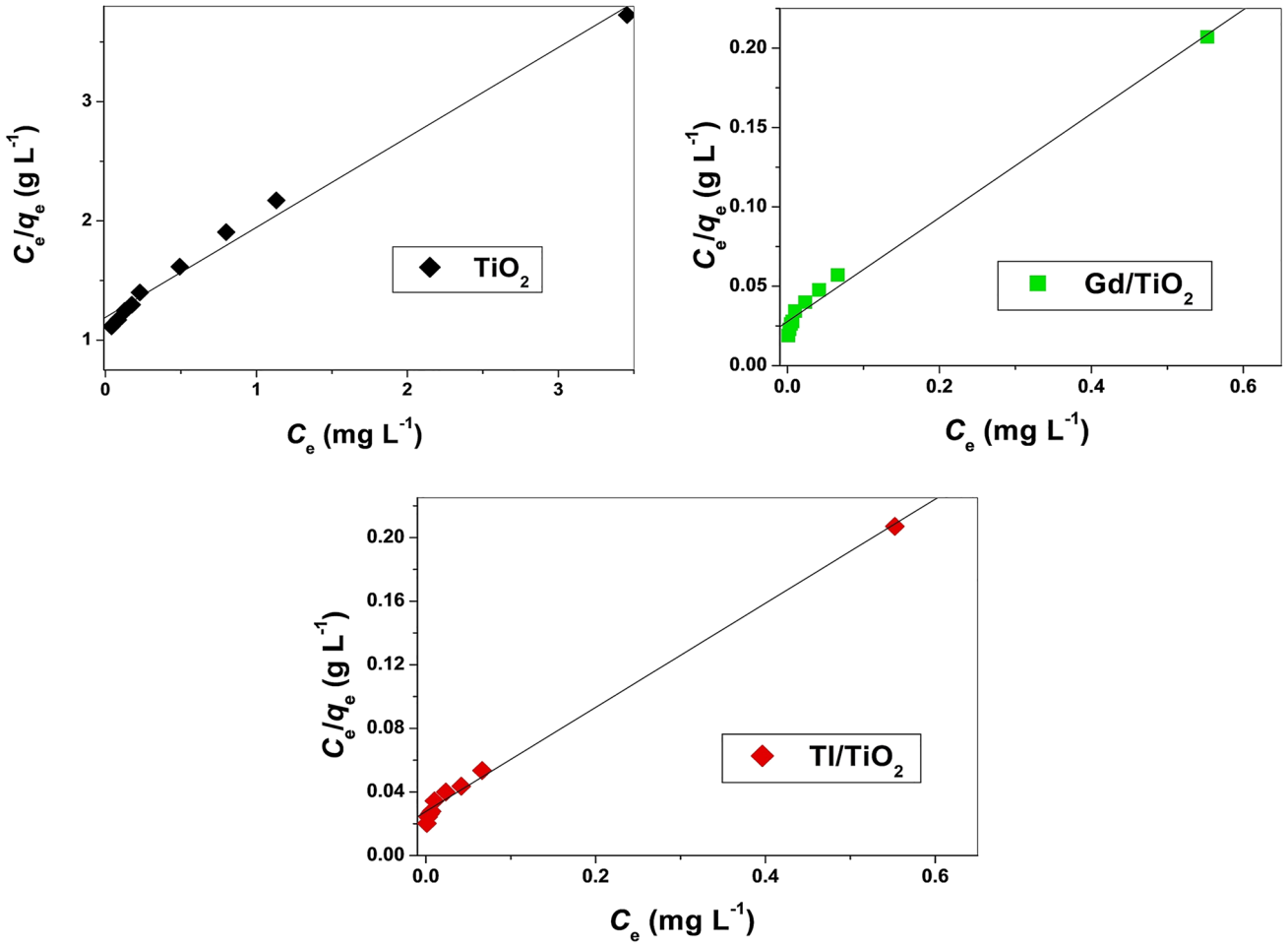

Fig. 6 Langmuir adsorption isotherm for the adsorption of As(III) onto pure and doped TiO_2 NPs

The linear fitting of models was examined by calculation of correlation coefficient (R^2). Similarly, the nearly close experiment and calculated maximum adsorption capacity (q_m, mg/g) values show that the Langmuir isotherm generates a satisfactory fit to the experimental data. The results suggest that the adsorption of As(III) ions by pure and doped-TiO_2 is monolayer-type and agrees with the observation that the adsorption from an aqueous solution usually forms a layer on the adsorbent surface.

Freundlich isotherm linear form of equation in logarithmic form is given as follow [15]:

$$\log q_e = \log K_F + 1/n \log C_e \quad (8)$$

where C_e (mg/L) is the amount of As(III) left in solution at equilibrium, q_e the adsorption capacity at equilibrium per unit weight of adsorbent (mg/g), and K_F and *n* are Freundlich constants. The plot of *log* C_e versus log q_e at various initial concentrations of As(III) was drawn for the pure and doped TiO_2 NPs. The *n* values (Table 3) ranged at 1.7 and 2.4 for pure and doped TiO_2 NPs indicating that the significant fraction of the As(III) mass was adsorbed instantaneously on adsorbents. However, the lower value R^2 (0.80–0.88), of pure and doped TiO_2 samples adsorption results do not match with Freundlich model.

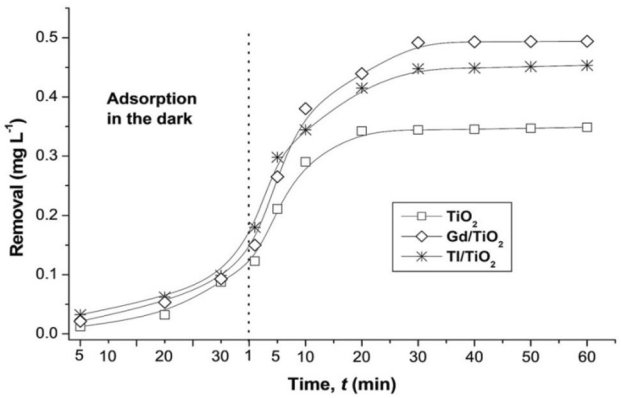

Fig. 7 Effect of contact time on the adsorption of As(III) using pure and doped TiO_2 NPs

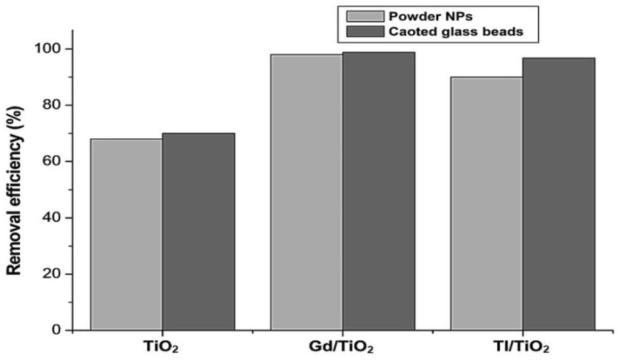

Fig. 8 Comparative As(III) removal efficiency onto powder and glass beads immobilized pure and doped TiO_2 NPs

4.3 Effect of contact time on the adsorption of As(III)

The effect of contact time was investigated for the adsorption of As(III) onto pure and doped TiO_2 NPs. Initial uptake of arsenic was higher due to the presence of large number of active sites on photocatalysts surface. It was observed that the system reached to equilibrium in first 30 to 35 min under compact fluorescent light (Fig. 7). Iervolino et al. [8] quoted that in photocatalytic process the initial As(III) oxidation was faster and almost total oxidation was observed after 60 min treatment. In present work for the doped TiO_2 NPs the adsorption rate was quite fast with almost 85% of As(III) removed in the initial 20 min, whereas the total removal was observed after 60 min. Furthermore, the results were obtained under neutral pH, typical for drinking water. The dark adsorptions were performed following same set of conditions in the dark for 30 min. Meanwhile, the removal efficiencies of pure and doped TiO_2 NPs were observed less than 20% in the dark.

4.4 Comparative removal efficiencies of powder and immobilized TiO_2 NPs

The comparative adsorption efficiency of As(III) onto powder as well as glass beads coated pure and doped TiO_2 NPs was investigated, as shown in Fig. 8. The results illustrate that the glass beads slightly enhanced the removal efficiencies of pure and Gd doped TiO_2 NPs, however, the enhancement in efficiency for immobilized Tl doped TiO_2 was more significant. The increased in the removal efficiency of immobilized Tl doped TiO_2 agrees with the EDX results, which showed that the degree of Tl doped TiO_2 coating on the surface of glass beads is higher than the other counterparts (Table 2).

The comparative efficiencies of powder and glass beads immobilized TiO_2 NPs were calculated for the removal of 5 ppm of As(III). The removal and percentage efficiencies trend is given as follow for powder samples; Gd/TiO_2 (4.90 ppm, 98%) > Tl/TiO_2 (4.51 ppm, 90%) > TiO_2 (3.43 ppm, 68%), respectively. However, for the immobilized samples the trend is, Gd/TiO_2 (4.94 ppm, 98.8%) > Tl/TiO_2 (4.82 ppm, 96.8%) > TiO_2 (3.50 ppm, 70%), respectively. Glass beads as a comparatively inexpensive inert solid support significantly overcome the post-reactions filtration/centrifugation steps. In addition, the slight but significant enhancement in the removal efficiency of in presence of inert support could be play a vital role in water treatment. The bare glass beads did not show any As(III) removal efficiency under same conditions.

Desorption studies were performed for spent powder and immobilized samples by agitating samples in distill water for 2 h. The desorption results indicated very small amount of arsenic desorption (~ 5–8 ppb) from the spent photocatalyst used for 5 ppm solution. However, the desorption from lower concentrations samples were negligible. The lower desorption from the spent photocatalysts used for highest concentration (5 ppm) As solution signposts the significance of photocatalysts for household drinking water treatments.

4.5 Regeneration

The high temperature combustion regeneration method is useful to recover the active site of photocatalysts. It was observed that the 1st cycle regenerated samples show the removal efficiencies near to fresh samples (as shown in Fig. 9). However, gradual decrease in efficiencies was observed for 2nd and 3rd cycles, which is due to the loss in active surface areas and agglomeration in aqueous medium. In addition, same trends of efficiencies were observed for immobilized samples.

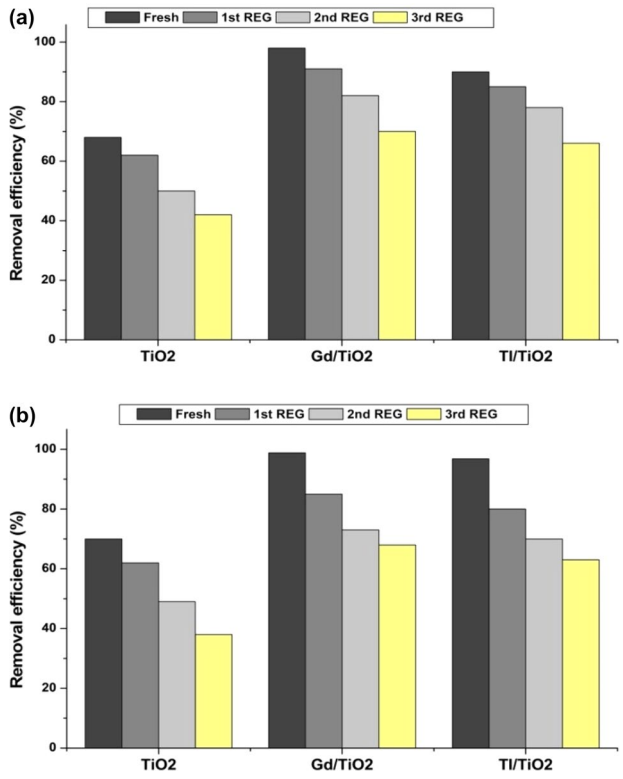

Fig. 9 Comparison of MB removal efficiency (%) of fresh and high temperature combustion regenerated **a** powder samples and **b** glass beads immobilized samples

5 Conclusions

Mesoporous Gd and Tl doped TiO_2 NPs prepared by liquid impregnation method showed different crystallite size and surface morphology. Both the doped systems used in this study were found in purely anatase phase with relatively high surface area and pore size compared to pure TiO_2. The annealing temperature (400 °C) and change in polarity by adding metal nitrate salts during preparation were assumed to be responsible for anatase structure formation. The surface area and tailoring of electronic properties by introducing metal cations as a guest phase increase the affinity of TiO_2 photocatalyst towards As(III) adsorption. The adsorption efficiencies results make it clear, that dopants have shift the adsorption wavelength of TiO_2 to visible region, as there are less than 20% adsorptions observed in the dark. This study concludes that the incorporations of dopants metals increases the photocatalytic activity of TiO_2 NPs under neutral pH (i.e. pH 7), compact fluorescent light and for minimum (ppb) to maximum (ppm) concentrations of As(III). The immobilization of TiO_2 NPs onto inert solid support (glass beads) not only makes significant contribution in enhancement of surface area and adsorption efficiencies but also overcome the post-reaction filtrations. The regeneration of both powder and immobilized samples could increase the effectiveness of photocatalyst for drinking and wastewater treatment technologies.

Acknowledgements The authors greatly acknowledge the support by Universiti Sains Malaysia (USM) and IESE, National University of Science and Technology (NUST), Pakistan. NS is also thankful to The World Academy of Sciences (TWAS) and USM for awarding the TWAS–USM Fellowship to pursue this study.

Compliance with ethical standards

Conflict of interest The authors declare that they have no conflict of interest.

References

1. Akter KF, Owens G, Davey DE, Naidu R (2005) Arsenic speciation and toxicity in biological systems. In: Ware GW et al (eds) Reviews of environmental contamination and toxicology. Springer, New York, pp 97–149
2. Bang S, Patel M, Lippincott L, Meng X (2005) Removal of arsenic from groundwater by granular titanium dioxide adsorbent. Chemosphere 60(3):389–397
3. Chen Y, Parvez F, Gamble M, Islam T, Ahmed A, Argos M, Garziano JH, Ahsan H (2009) Arsenic exposure at low-to-moderate levels and skin lesions, arsenic metabolism, neurological functions, and biomarkers for respiratory and cardiovascular diseases: review of recent findings from the Health Effects of Arsenic Longitudinal Study (HEALS) in Bangladesh. Toxicol Appl Pharmacol 239(2):184–192
4. Clancy TM, Hayes KF, Raskin L (2013) Arsenic waste management: a critical review of testing and disposal of arsenic-bearing solid wastes generated during arsenic removal from drinking water. Environ Sci Technol 47(19):10799–10812
5. Danish MI, Qazi IA, Zeb A, Habib A, Ali Awan M, Khan Z (2013) Arsenic removal from aqueous solution using pure and metal-doped titania nanoparticles coated on glass beads: adsorption and column studies. J Nanomater 2013:69
6. Deedar N, Aslam I (2009) Evaluation of the adsorption potential of titanium dioxide nanoparticles for arsenic removal. J Environ Sci 21(3):402–408
7. Gaya UI (2011) Comparative analysis of ZnO-catalyzed photooxidation of p-chlorophenols. Eur J Chem 2(2):163–167
8. Iervolino G, Vaiano V, Rizzo L, Sarno G, Farina A, Sannino D (2016) Removal of arsenic from drinking water by photo-catalytic oxidation on MoOx/TiO_2 and adsorption on γ-Al_2O_3. J Chem Technol Biotechnol 91(1):88–95
9. Islam M, Patel R (2007) Evaluation of removal efficiency of fluoride from aqueous solution using quick lime. J Hazard Mater 143(1):303–310
10. Izadyar S, Fatemi S (2013) Fabrication of X zeolite based modified nano TiO_2 photocatalytic paper for removal of VOC pollutants under visible light. Ind Eng Chem Res 52(32):10961–10968
11. Jezequel H, Chu K (2006) Removal of arsenate from aqueous solution by adsorption onto titanium dioxide nanoparticles. J Environ Sci Health Part A 41(8):1519–1528
12. Khataee A (2009) Photocatalytic removal of CI Basic Red 46 on immobilized TiO_2 nanoparticles: artificial neural network modelling. Environ Technol 30(11):1155–1168

13. Korte NE, Fernando Q (1991) A review of arsenic(III) in groundwater: critical reviews. Environ Sci Technol 21(1):1–39
14. Lee H, Choi W (2002) Photocatalytic oxidation of arsenite in TiO_2 suspension: kinetics and mechanisms. Environ Sci Technol 36(17):3872–3878
15. Lee Y-C, Yang J-W (2012) Self-assembled flower-like TiO_2 on exfoliated graphite oxide for heavy metal removal. J Ind Eng Chem 18(3):1178–1185
16. Liu G, Zhu D, Liao S, Ren L, Cui J, Zhou W (2009) Solid-phase photocatalytic degradation of polyethylene–goethite composite film under UV-light irradiation. J Hazard Mater 172(2):1424–1429
17. Liu R, Wu H, Yeh R, Lee C, Hung Y (2012) Synthesis and bactericidal ability of TiO_2 and Ag-TiO_2 prepared by coprecipitation method. Int J Photoenergy 2012:640487
18. Miller SM, Zimmerman JB (2010) Novel, bio-based, photoactive arsenic sorbent: TiO_2-impregnated chitosan bead. Water Res 44(19):5722–5729
19. Parida K, Sahu N (2008) Visible light induced photocatalytic activity of rare earth titania nanocomposites. J Mol Catal A Chem 287(1):151–158
20. Rizzo L, Lofrano G, Grassi M, Belgiorno V (2008) Pre-treatment of olive mill wastewater by chitosan coagulation and advanced oxidation processes. Sep Purif Technol 63(3):648–653
21. Saqib NU, Adnan R, Shah I (2016) A mini-review on rare earth metal-doped TiO_2 for photocatalytic remediation of wastewater. Environ Sci Pollut Res 23(16):15941–15951
22. Saqib NU, Adnan R, Shah I (2019) Zeolite supported TiO_2 with enhanced degradation efficiency for organic dye under household compact fluorescent light. Mater Res Express 6(9):095506
23. Sharma VK, Sohn M (2009) Aquatic arsenic: toxicity, speciation, transformations, and remediation. Environ Int 35(4):743–759
24. Shi J, Zheng J, Wu P, Ji X (2008) Immobilization of TiO_2 films on activated carbon fiber and their photocatalytic degradation properties for dye compounds with different molecular size. Catal Commun 9(9):1846–1850
25. Smedley P, Nicolli H, Macdonald D, Barros A, Tullio J (2002) Hydrogeochemistry of arsenic and other inorganic constituents in groundwaters from La Pampa, Argentina. Appl Geochem 17(3):259–284
26. Su H, Lv X, Zhang Z, Yu J, Wang T (2017) Arsenic removal from water by photocatalytic functional Fe_2O_3–TiO_2 porous ceramic. J Porous Mater 24(5):1227–1235
27. Valencia S, Marín JM, Restrepo G (2010) Study of the bandgap of synthesized titanium dioxide nanoparticules using the sol–gel method and a hydrothermal treatment. Open Mater Sci J 4(1):9–14
28. Wei H, Wu Y, Lun N, Zhao F (2004) Preparation and photocatalysis of TiO_2 nanoparticles co-doped with nitrogen and lanthanum. J Mater Sci 39(4):1305–1308
29. Zhao L, Cui T, Li Y, Wang B, Han J, Han L, Liu Z (2015) Efficient visible light photocatalytic activity of p–n junction CuO/TiO_2 loaded on natural zeolite. RSC Adv 5(79):64495–64502